Graphene-Based Interfaces Do Not Alter Target Nerve Cells

Alessandra Fabbro,[†,‡] Denis Scaini,[†,§,‖] Verónica León,[⊥] Ester Vázquez,*[,⊥] Giada Cellot,[†] Giulia Privitera,[#] Lucia Lombardi,[#] Felice Torrisi,[#] Flavia Tomarchio,[#] Francesco Bonaccorso,[#,∇] Susanna Bosi,[‡] Andrea C. Ferrari,*[,#] Laura Ballerini,*[,†,§] and Maurizio Prato*[,‡,¶,○]

[†]International School for Advanced Studies (SISSA/ISAS), Trieste 34136, Italy

[‡]Department of Chemical and Pharmaceutical Sciences, University of Trieste, Trieste 34127, Italy

[§]Life Science Department, University of Trieste, Trieste 34127, Italy

[‖]NanoInnovation Laboratory, ELETTRA Synchrotron Light Source, Trieste 34149, Italy

[⊥]Department of Organic Chemisty, University of Castilla-La Mancha, Ciudad Real 13071, Spain

[#]Cambridge Graphene Centre, University of Cambridge, Cambridge CB3 0FA, United Kingdom

[∇]Istituto Italiano di Tecnologia, Graphene Labs, Genova 16163, Italy

[¶]Carbon Nanobiotechnology Laboratory, CIC biomaGUNE, Paseo de Miramón 182, 20009 Donostia-San Sebastian, Spain

[○]Basque Foundation for Science, Ikerbasque, Bilbao 48013, Spain

S Supporting Information

ABSTRACT: Neural-interfaces rely on the ability of electrodes to transduce stimuli into electrical patterns delivered to the brain. In addition to sensitivity to the stimuli, stability in the operating conditions and efficient charge transfer to neurons, the electrodes should not alter the physiological properties of the target tissue. Graphene is emerging as a promising material for neuro-interfacing applications, given its outstanding physico-chemical properties. Here, we use graphene-based substrates (GBSs) to interface neuronal growth. We test our GBSs on brain cell cultures by measuring functional and synaptic integrity of the emerging neuronal networks. We show that GBSs are permissive interfaces, even when uncoated by cell adhesion layers, retaining unaltered neuronal signaling properties, thus being suitable for carbon-based neural prosthetic devices.
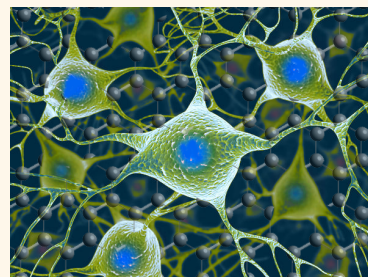
KEYWORDS: hippocampal cultures, synaptic networks, neuronal interfaces, graphene, liquid phase exfoliation, patch clamp

Coupling (nano)materials to organic tissues is crucial for developing prosthetic applications, where the interfacing surfaces should provide minimal undesired disturbance to the target tissue.[1] Ultimately, the (nano)material of choice has to be biocompatible,[1,2] promoting cellular growth and adhesion with minimal cytotoxicity or dysregulation of, e.g., cellular activity.[2]

In neurology, relevant examples in the area of prosthetic devices are deep-brain intracranial electrodes,[3] used to control motor disorders, or brain interfaces, such as those used to recover sensory functions[4] or to control robotic arms for amputated patients.[5] In all these cases, the inorganic material constituting the interfaced electrode has to preserve unaltered tissue functionality to avoid uncontrolled side effects.[5] A charge transfer taking place from electrodes to neurons, flexibility and ease of molding into complex shapes are also key requirements.[2] Current approaches involve the use of tungsten microwire electrodes,[6] or silicon based electrode arrays.[6] The clinical relevance of these approaches has been demonstrated.[4] However, drawbacks are still limiting their long-term performance when implanted.[1] The most common is the formation of an insulating layer around the electrodes, the so-called "glial scar",[7] as a consequence of insertion-related brain trauma and long-term inflammation. This can halve the level of the desired signal (electrical stimulus delivered/recorded by the electrode) with respect to the level of background noise, namely the signal-to-noise ratio,[1,7] leading to electrode failure.[6] Another failure mechanism stems from the electrodes' stiffness, usually larger than the surrounding tissue, resulting in tissue detachment.[1] Thus, there is a need to develop flexible electrodes, consisting of biocompatible, cell-adhesion-promoting and conductive materials.

Carbon-based nanomaterials, such as carbon nanotubes (CNTs), have been extensively used as neural electrodes.[1,8−15] Interfacing neurons with CNTs was shown to increase neuronal activity, at least *in vitro*, in various experimental models.[8,16−20]

1

This can be exploited in neural prostheses/devices to bypass nonfunctional neuronal tissue (e.g., glial scar following a lesion).[21] Coating extracellular electrodes with CNTs enhances both recording and electrical stimulation of neurons, both in-culture and in vivo, in rats and monkeys, by decreasing the electrode impedance and increasing charge transfer.[9] CNTs can also alter the neuronal behavior in terms of spontaneous synaptic activity[16] and action potential firing frequencies.[16] Neuroprosthetics applications require low neuronal tissue perturbation:[1] implanted electrodes must excite the neuronal cells, without depressing (or boosting) the surrounding neuronal network.[1]

Due to its excellent electrical properties,[22] graphene is promising for the development of neural interfaces.[23,24] A number of studies to date have addressed the issue of graphene toxicity.[24,25] However, less attention was paid to graphene biointerfaces, in particular those exploiting nonchemically-modified graphene,[26,27] and even fewer reports have addressed the issue of biocompatibility with neuronal cells.[28,30] Polylysine-covered graphene was shown[28] to be a neuro-favorable laminar material, sustaining viability and improving the growth of specialized neuronal compartments (the neuritis) in dissociated hippocampal cultures.[28] Laminin-coated graphene favors the differentiation of neural stem cells into neurons.[31] However, peptide-based (e.g., polylysine or polyornithine) coatings might increase the electrical resistance of the neuron/interface electrical contacts, thus affecting the charge transfer properties.[28,32,3]The direct contact and exposure of neurons to GBSs is crucial to promote tight adhesion between cell membranes and interfacing electrodes, a key requirement to detect small (tens of μV^9) signals during extracellular recordings, and to reduce voltage drops during tissue stimulation, thus improving charge transfer.[28,32−34] Reference 28 reported the biocompatibility of uncoated graphene surfaces with neuronal cells in terms of neuronal survival and morphology. However, to the best of our knowledge, thus far no study addressed how uncoated graphene may impact the neuronal electrophysiological behavior.

Micromechanical exfoliation can be used to produce graphene flakes with outstanding structural and electronic properties.[35−39] However, its limited yield makes it impractical for large-scale applications.[36] Graphene films can be produced by carbon segregation from metal substrates[40,41] or SiC[42,43] or by chemical vapor deposition[44,45] followed by transfer (wet[36] or dry[45]) to a target substrate.[36] However, such processes require high temperatures (>1000 °C),[36,45−47] costly substrates, besides the additional transfer.[36] Solution processing is emerging as a most promising technique to produce single- (SLG) and few-layer (FLG) graphene flakes on a large scale,[36] both starting from oxidized[48−51] and pristine graphite.[36,52−58] Graphene oxide (GO), produced by exfoliation of graphite oxide, can be mass-produced at room temperature.[48,49] However, it is insulating,[49,50] with defects[49,50] and gap states,[50,51] and may not offer the optimal charge transfer between substrate and neurons.[36] Liquid phase exfoliation (LPE) of graphite[52] can be performed without the potentially hazardous chemical treatments involved in GO production,[48−51] being at the same time scalable, room temperature and high yield.[36] LPE dispersions can also be easily deposited on target substrates, by drop casting,[53] filtration[52] or printing.[54] Another approach to graphite exfoliation is ball milling (BM) with the help of melamine, which forms large H-bond domains and intercalates graphite[55,56] and, unlike LPE, can be performed in solid.[56]

Here, we use LPE and BM of graphite to fabricate GBSs. Electrophysiological measurements show the biocompatibility in vitro of both samples with dissociated hippocampal neuronal cultures. Our GBSs allow neuronal adhesion and growth when mammalian, differentiated, postmitotic neurons are explanted and cultured on them. We also investigate the impact on neuronal, synaptic and network electrophysiological properties, to address the ability of our GBSs to interface and transform neuronal signaling.[59] We find that our GBSs favor nerve-cell adhesion and survival without altering the cell differentiation, biophysics passive properties, synaptogenesis, spontaneous synaptic activity and plasticity, when compared to control growth-substrates. Our GBSs also retain neuronal signaling properties, thus paving the way to the development of carbon-based neural interfaces able to preserve the neuronal activity.

RESULTS AND DISCUSSION

The GBSs are produced following two different protocols, LPE and BM, in order to unveil possible effects of materials production, processing, deposition and structure, on neuronal activity.

The LPE protocol is as follows: 120 mg of graphite flakes (Sigma-Aldrich) are dispersed in 10 mL of deionized water (DIW) with 90 mg of sodium deoxycholate (SDC), then placed in an ultrasonic bath for 9 h and subsequently ultracentrifuged exploiting sedimentation-based separation (SBS)[36] using a TH-641 swinging bucket rotor in a Sorvall WX-100 ultracentrifuge at 10 krpm ($\sim$17 000g) for 1 h. After ultracentrifugation, the top 70% of the dispersion is extracted by pipetting and deposited on glass coverslips by vacuum filtration and film transfer. The dispersion is characterized by optical absorption spectroscopy (OAS) and Raman spectroscopy. OAS of the dispersions, diluted to 10% to avoid scattering losses at higher concentrations, is acquired in the range 200−1300 nm with a PerkinElmer Lambda 950 spectrophotometer. The concentration of graphitic flakes is determined from the optical absorption coefficient at 660 nm, using $A = \alpha l c$ where l [m] is the light path length, c [g L^{-1}] is the concentration of dispersed graphitic material, and α [L g^{1-} m^{-1}] is the absorption coefficient, with $\alpha \sim 1390$ L g^{1-} m^{-1} at 660 nm.[52,54] For Raman spectroscopy, the dispersions are drop-cast onto a Si wafer with 300 nm thermally grown SiO$_2$ (LDB Technologies Ltd.), dried on a hot plate and rinsed in a solution of DIW/ethanol (50:50). Raman measurements on both the graphene dispersions and GBSs are collected using a Renishaw InVia spectrometer at 457, 514.5, and 633 nm with a 100× objective and an incident power <1 mW. The G peak dispersion is defined as Disp(G) = ΔPos(G)/$\Delta\lambda_L$, where Pos(G) is the position of the G peak, λ_L is the laser excitation wavelength, and Δ indicates the rate of change of Pos(G) as a function of varying λ_L.

LPE-GBSs dispersions are then vacuum filtered via 100 nm pore-size filters (Millipore nitrocellulose filter membranes). This blocks flakes, while allowing water to pass through. To remove the residual surfactant, the GBSs deposited on the filters are rinsed by vacuum filtration of 20 mL DIW. The film transfer on glass coverslips is done by applying pressure and heat ($\sim$90 °C, to improve adhesion) overnight ($\sim$10 h), followed by dissolution of the filter in acetone. The GBSs are then rinsed in isopropyl alcohol and in DIW baths, and finally dried in oven ($\sim$90 °C) for 1 h.

The BM-GBSs are produced by exfoliation of graphite (from Bay Carbon) with melamine,[55] and then dispersed in dimethylformamide (DMF), followed by drop casting on glass coverslips placed on a hot plate at 100 °C. The substrates are thermally treated for 20 min in an oven at 350 °C under nitrogen atmosphere to remove traces of solvent or impurities.
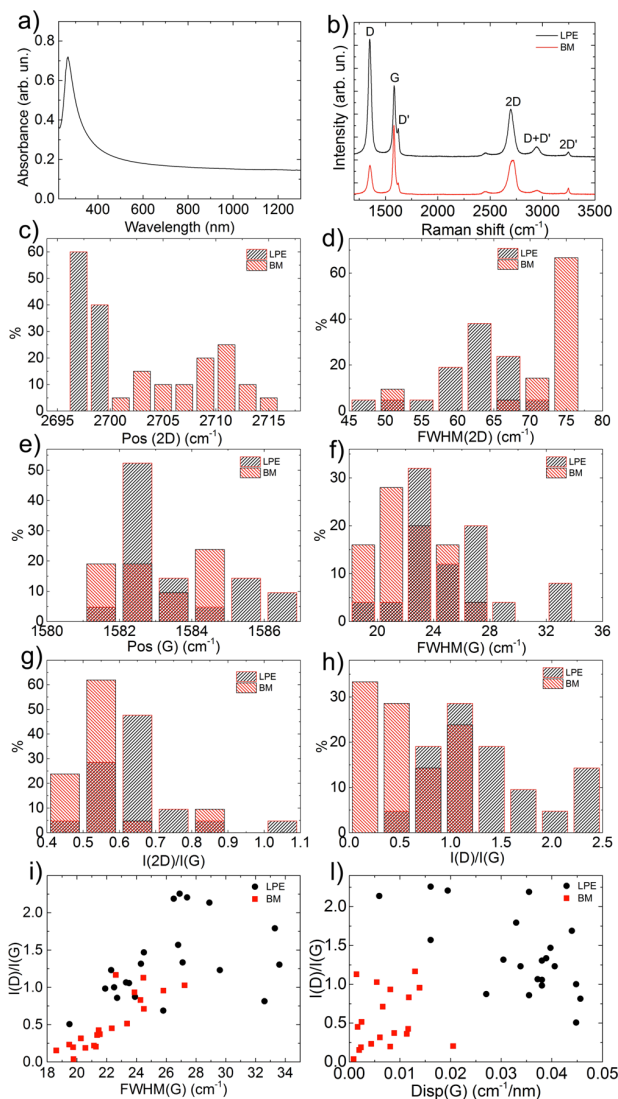
Figure 1. (a) Optical absorption of LPE dispersion diluted 1:12 with pure water/SDC. (b) Raman spectrum at 514.5 nm for representative LPE (black curve) and BM (red curve) flakes. Distribution of (c) Pos(2D), (d) FWHM(2D), (e) Pos(G), (f) FWHM(G), (g) $I(2D)/I(G)$, (h) $I(D)/I(G)$, and distribution of $I(D)/I(G)$ as a function of (i) FWHM(G) and (l) Disp(G) for LPE (black dashed histograms and dots) and BM (red dashed histograms and dots) flakes, respectively.

Figure 1a plots the absorbance of the LPE dispersion. The peak at ~266 nm is a signature of the van Hove singularity in the graphene density of states.[60] Figure 1b plots a typical Raman spectrum (black curve) measured at 514.5 nm of representative flakes of the LPE dispersion on Si/SiO$_2$. The G peak corresponds to the E$_{2g}$ phonon at the Brillouin zone center.[60] The D peak is due to the breathing modes of sp^2 rings and requires a defect for its activation by double resonance (DR).[62−64] The 2D peak is the second order of the D peak.[63] This is a single peak in SLG, whereas it splits in FLG, reflecting the evolution of the band structure.[62] The 2D peak is always seen, even when no D peak is present, since no defects are required for the activation of two phonons with the same momentum, one backscattered from the other.[61] DR can also

happen as intravalley process, *i.e.*, connecting two points belonging to the same cone around **K** or **K**′.[62] This process gives rise to the D′ peak. The 2D′ is the second order of the D′. Statistical analysis (black dashes plots), based on 30 measurements for each excitation wavelength (457, 514.5, 633 nm), gives an average position of the 2D peak, Pos(2D), ~2698 cm^{-1} (Figure 1c). FWHM(2D) varies from 45 to 72 cm^{-1} (Figure 1d) with a peak at ~63 cm^{-1}. Pos(G), Figure 1e, and FWHM(G), Figure 1f, are 1583 and 24 cm^{-1}. $I(2D)/I(G)$ ranges from 0.4 to 1.1 (Figure 1g). This is consistent with the samples being a combination of SLG and FLG flakes. The Raman spectra show significant D and D′ peaks intensity, with $I(D)/I(G)$ ranging from 0.5 to 2.5 (Figure 1h). This is attributed to the edges of our submicrometer flakes,[65] rather than to the presence of a large amount of structural defects within the flakes. This observation is supported by the low Disp(G) < 0.05 cm^{-1}/nm, much lower than what expected for disordered carbon.[63,64] Combining $I(D)/I(G)$ with Disp(G) allows us to discriminate between disorder localized at the edges and disorder in the bulk. In the latter case, a higher $I(D)/I(G)$ would correspond to higher Disp(G) (see Figure 1l). The lack of a clear correlation between $I(D)/I(G)$ and FWHM(G) (see Figure 1i) is an indication that the major contribution to the D peak comes from the sample edges.

Similarly to LPE, Figure 1b plots a typical Raman spectrum (red curve) measured at 514.5 nm of representative BM flakes on Si/SiO$_2$. A statistical analysis based on 30 measurements for each excitation wavelength (457, 514.5, 633 nm) gives an average Pos(2D) ~ 2708 cm^{-1} (Figure 1c) and FWHM(2D) peaked at 75 cm^{-1} (Figure 1d). Pos(G), Figure 1e, and FWHM(G), Figure 1f, are 1583 and 22 cm^{-1}. $I(2D)/I(G)$ peaks at ~0.5 (Figure 1g) . The Raman spectra show lower $I(D)/I(G)$ and $I(D')/I(G)$ than the LPE samples, with $I(D)/I(G)$ having a bimodal distribution peaked at 0.2 and 1.0 (Figure 1h). However, the correlation between $I(D)/I(G)$ and FWHM(G), Figure 1i, indicates that defects are present inside the samples, and that the D peak does not only come from the edges. The comparison between the Raman data on LPE and BM samples indicates that the latter mostly comprise defective graphite flakes a few layer thick, while the former mostly consist of SLG, or FLG, but electronically decoupled, and with fewer defects.

Before cell deposition, both LPE and BM-GBSs are thermally annealed for 20 min at 350 °C in nitrogen in order to remove residual solvent. Electrical measurements show that for LPE-GBSs, the sheet resistance, R_s, is ~3.4 kΩ/□, which corresponds, using $R_s = 1/\sigma t$ [with t ~ 150 nm], to an average value of conductivity (σ) 2600 ± 400 S/m, comparable with other films produced by LPE graphene[36] and reduced GO (σ ~ 10^3 S/m).[66] The BM-GBSs have a lower σ = 1010.1 ± 90.0 S/m with respect to the LPE-GBSs.

Figure 2a compares 514.5 nm representative Raman spectra for LPE and BM dispersions with the spectra of the resulting LPE-GBS and BM-GBS after annealing. Figure 2b−e compares the distribution of Pos(2D) and FWHM(2D). The LPE-GBS has a narrower distribution of both Pos(2D) (peak at ~2698 cm^{-1}) and FWHM(2D) (peak at ~72 cm^{-1}), with respect to the LPE dispersion. However, the 2D peak still shows a Lorentzian line shape distinctly different from that of graphite. The BM-GBS has a similar distribution of both Pos(2D) (ranging from ~2698 to 2718 cm^{-1}) and FWHM-(2D) (peak at ~85 cm^{-1}), to those of the BM dispersion and the 2D peak line shape indicates the predominance of thick flakes.
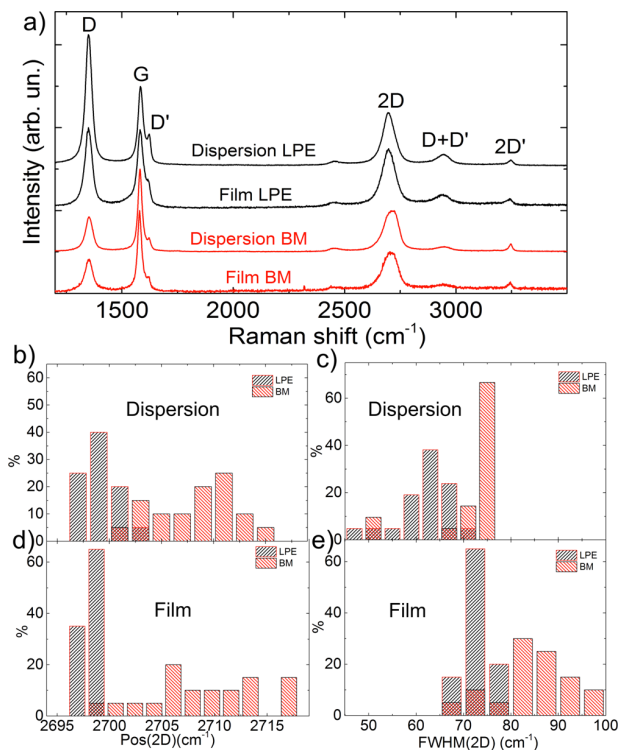
Figure 2. (a) Representative Raman spectra of flakes, compared with films. LPE (black curve) and BM (red curve). Pos(2D) and FWHM(2D) for (b and c) flakes in dispersion and (d and e) films deposited on glass substrates for LPE (black dashed histograms) and BM (red dashed histograms).

AFM measurements are also used to characterize the GBSs. They are carried out with a Bruker Dimension Icon equipped with NanoScope V Controller in ScanAsyst PeakForce Tapping Mode using ScanAsyst-Air Silicon Nitride probes with a nominal tip radius of 2 nm. Topographic images are taken on surface areas of 100 μm^2 to measure roughness, while 80 μm profiles across the film edges are used to estimate the thickness.[67] Figure 3a shows an average root means square (RMS) roughness of 14.1 ± 2.9 nm and roughness average (Ra) of 9.0 ± 1.4 nm, with an average film thickness (t) of 131 ± 44 nm. The BM-GBS shows a sub-micrometric morphology, with the lateral dimensions of the flakes <200 nm (Figure 3b).

Following the structural characterization, neuronal cultures are placed on the GBSs and electrophysiology studies are performed as detailed in Methods. Both peptide-free and polyornithine-covered glass coverslips are used as control substrates. We design the first set of experiments (reported in details in the Supporting Information) to separately compare the ability of the different GBS substrates, prepared from LPE and BM, to interface and allow neuronal network formation *in vitro*. Thus, we preliminarily match (Supporting Information and Figures S1 and S2) sample cultures grown on the LPE or on the BM-GBSs with their respective control substrates. To examine neuronal cells when interfaced to the various substrates, we compare their membrane passive properties, *i.e.*, the input resistance and cell capacitance (Figure S1), which are also indicative of neuronal health conditions.[59] In individual data-set, neurons grown on LPE or on BM are measured against their control sister cultures (*i.e.*, within the same culture series) and these results show that both tested GBSs conditions

allow neuronal growth without apparent differences with controls in the measured parameters (Figure S1 and S2). The detected membrane passive properties are in agreement with previous control assessments for hippocampal neurons in culture.[8,17,18] Thus, data on both GBSs and on pure glass or polyornithine-covered glass are pooled and collectively named GBSs or control, respectively.

Neurons are investigated by electron microscopy and immunofluorescence. They show normal morphology characterized by well-defined round soma and extended neurite arborization (Figure 3c) and a cell density similar to control substrates. The density of neuronal cells, quantified by staining neuronal nuclei with the specific marker NeuN, is 91 ± 13 neurons/mm^2 on the control substrate and 104 ± 11 cells/mm^2 on GBSs (immunofluorescence shown for control (Figure 3d) and LPE-GBS (Figure 3e)). Figure 3f plots the neuronal density for GBSs pooled data ($n = 12$ fields from 4 cultures). Similarly, the growth of glial cells, identified by their marker glial fibrillary acidic protein, GFAP, is unaffected by both GBSs. The glial cells density is 84 ± 5 cells/mm^2 on the control substrate and 100 ± 8 cells/mm^2 on GBSs (immunofluorescence shown for control (Figure 3g) and LPE-GBS (Figure 3h)). Figure 3i shows the glial cell density in the GBSs culture condition pooled data ($n = 12$ fields from 4 cultures).

It is important to test whether graphene affects the network synaptic behavior, since this is predictive of information processing,[17] in view of developing biocompatible GBSs able to fully preserve neuronal functionality. To this aim, we analyze both spontaneous network activity and neuronal synaptic connectivity in cultures developed on GBSs or on control substrates. Figure 4a,b shows typical heterogeneous spontaneous postsynaptic currents (PSCs) recorded from a voltage-clamped control neuron (Figure 4a) and from neurons grown onto the GBSs surface (Figure 4b). Graphene interfacing does not affect the frequency of spontaneous PSCs (4.0 ± 0.9 Hz, $n = 25$ and 3.6 ± 0.8 Hz, $n = 21$, for control and GBSs cultures, respectively; Figure 4c) and their amplitude (51 ± 7 pA for controls and 54 ± 6 pA for GF, respectively; Figure 4d). The network sizes of graphene-interfaced and control cultures are similar, as indicated by the comparable neuronal density, consequently they contribute equally to the PSC frequencies. GBS interfaces do not alter the spontaneous PSC frequency. This is further supported by the results shown in Figure S2 where we measure PSCs in sampled cultures individually (LPE or BM). The observation that GBSs are inert growth substrates to synaptic networks is also strengthened by an additional set of experiments where we interface neurons to multiwall carbon nanotubes (MWNTs). In the same cultures series we compare the frequency of PSCs of MWNTs, GBSs and control growth substrates (Supporting Information and Figure S3). We measure a selective increase in activity only in MWNT neurons (Figure S3), confirming the reported[8,16−20] ability of MWNTs to boost synaptic activity. This differs from that reported in ref 30, where graphene induced the enhancement of electrical signaling in the neural network. However, we believe that the results in ref 30 are, at least in part, biased by the presence of different network sizes in the two culturing conditions.

We then indirectly measure the impact of GBSs on the *in vitro* formation of functional contacts (*i.e.*, synaptogenesis) by simultaneously patch clamping randomly selected neuron pairs,[18] see Figure 5a. In each cell pair, an action potential is elicited in the presynaptic neuron, and the presence of a monosynaptic connection between the two neurons is assessed
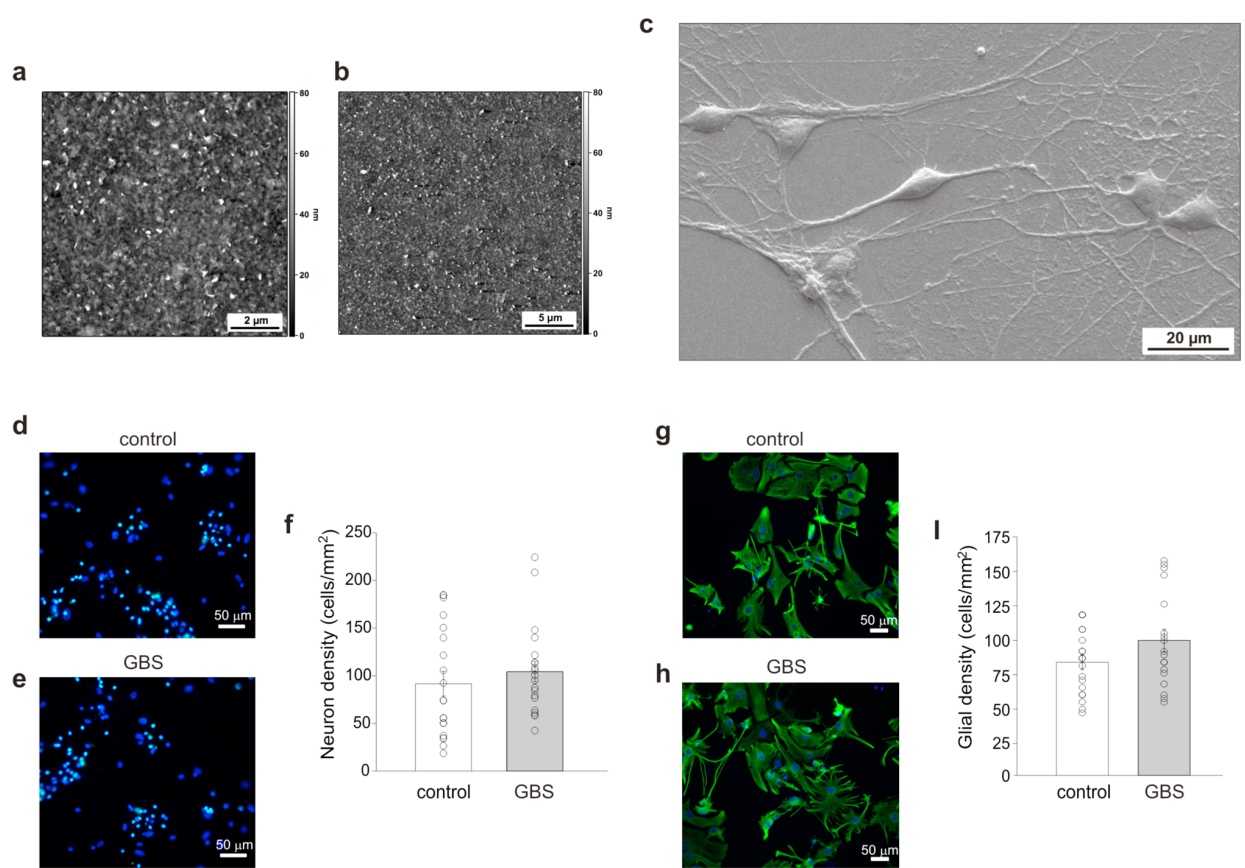
Figure 3. AFM images of (a) LPE-GBS and (b) BM-GBS. (c) SEM image of dissociated hippocampal neurons grown onto LPE-GBS. Immunofluorescence staining of cultures developed on (d) control and (e) LPE-GBS substrates, marked for neurons (NeuN, green) and nuclei (DAPI, blue). (f) Plot summaries of neuronal density in the two GBSs culturing conditions. Immunofluorescence staining for glial cells (marked for GFAP, green; DAPI in blue) on (g) control and (h) LPE-GBS. (i) Plot summaries of glial cells density in the two GBSs culturing conditions. Histograms are mean $\pm$ standard error.
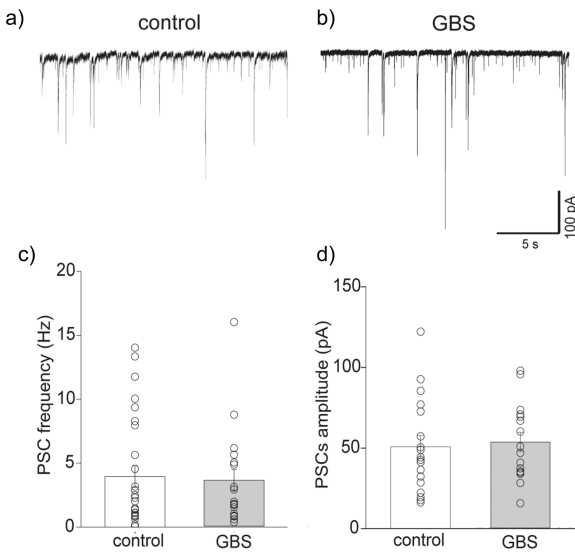

Figure 4. Representative PSC current tracings recorded from voltage clamped neurons grown on (a) control substrates or on (b) LPE-GBS. Frequency and amplitude of spontaneous PSCs are almost identical in neurons grown on (c) control and on (d) GBSs. Each dot represents values from a single neuron. Histograms are mean $\pm$ standard error.

by the PSC response in the postsynaptic neurons. The probability of finding monosynaptically coupled neurons pairs (expressed as %) is a measure of functional synaptic connections formed in the in vitro network.[18] We observe a % pairing on GBSs similar to that found on control substrates (29 $\pm$ 10% and 39 $\pm$ 11%, n = 5 culture series; total n = 30 pairs on GBSs and n = 28 pairs on control substrate), thus indicating that GBSs interfacing does not alter synaptogenesis, see Figure 5b. No differences in the amplitude of induced presynaptic action potentials are found between neurons in control and GBSs (91 $\pm$ 9 mV, n = 10 cells in control and 93 $\pm$ 4 mV, n = 11 cells on GBS, P = 0.7).

We then investigate the short-term synaptic plasticity, by eliciting a pair of action potentials in the presynaptic neuron (at 20 Hz), measuring the amplitude of the evoked PSCs in the postsynaptic neuron (Figure 5c,d), and evaluating the ratio between the amplitudes of the second and first PSCs in the pair (paired-pulse ratio, Figure 5e). We find a moderately depressing response (paired-pulse ratio 0.89 $\pm$ 0.07, n = 9 pairs) in the control, very similar to GBSs (paired-pulse ratio 0.86 $\pm$ 0.10, n = 7 pairs; amplitude of the first PSC 36 $\pm$ 6 pA, n = 10 and 44 $\pm$ 9, n = 8 for control and GBS substrates, respectively).

The observation that GBSs support neuronal functional development in the absence of any perturbation of neuronal network synaptic performance is intriguing. Other electrical conductive carbon-based nanomaterials, such as CNTs, are known[16,19] for their ability to reshape spontaneous network
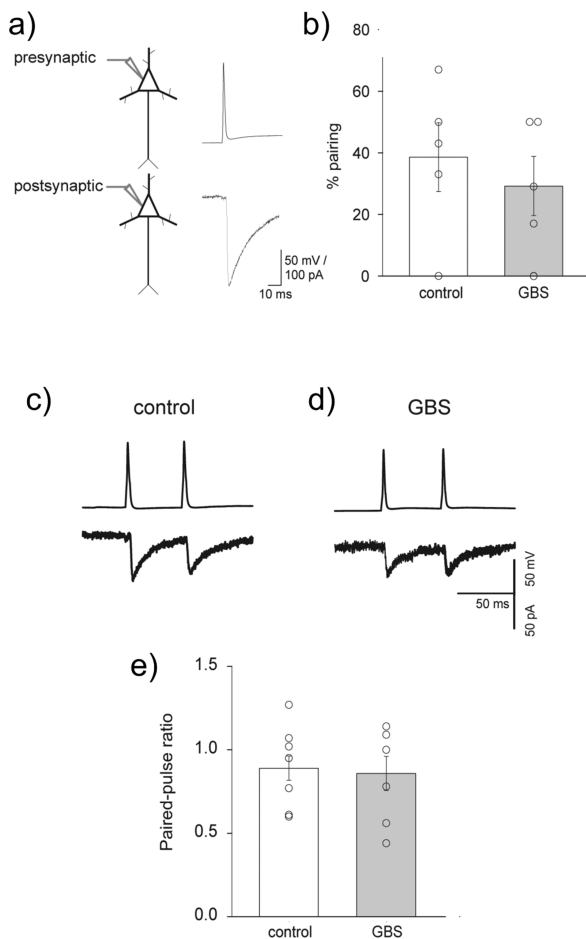
Figure 5. (a) Schematic representation of the experimental setting of dual recordings: an action potential is elicited in the presynaptic neurons (current-clamped; top), while recording response post-synaptic current from the postsynaptic neurons (voltage-clamped, bottom). (b) The fraction of synaptically coupled neuron pairs is similar in the two culturing conditions. Each dot represents the % pairing from neurons recorded from the same culture series. Dual recordings from neurons interfaced to (c) control or (d) BM-GBS substrates, in which a pair of action potentials at 20 Hz is induced in the presynaptic neurons (top traces) and the response postsynaptic current recorded in the postsynaptic neurons (bottom traces), to investigate short-term synaptic plasticity (paired pulse). The action potentials pair decrease the amplitude of the second postsynaptic current with respect to the first one (paired pulse depression) in both control and GBSs-interfaced neurons. (e) Histograms quantifying synaptic plasticity as the ratio between the amplitudes of the second and first postsynaptic currents (paired-pulse ratio). Each dot represents the value from one neuron pair. Histograms are mean ± standard error.

explain their inert nature in spite of their high electrical conductivity.

CONCLUSIONS

Our data show that GBSs, produced by liquid phase exfoliation or ball milling of graphite, are inert neuron-interfacing materials, able to preserve the basal physiological level of neuronal activity. The ability to interface neuronal circuit regrowth without altering cell and synapse behavior may enable the fabrication of graphene-based devices for medical applications,[25] such as biosensors[25] and neuroprosthetics,[23] whereby GBSs at the tissue interface result in efficient interaction with cells. In the future design of electrically functional implants, the use of novel materials characterized by the ability to integrate with tissue and, at the same time, flexible and not affecting excitable tissue behavior, is highly relevant. Our data indicate that both GBSs are promising for next generation bioelectronic systems, to be used as brain-interfaces. In this framework, it is important to note the uncommon ability of our GBSs to support neuronal development (in terms of neuronal passive properties, spontaneous synaptic activity, synaptogenesis, and short-term synaptic plasticity) without precoating with adhesion-promoting peptides (e.g., polylysine or polyornithine). Previous works demonstrated the full biocompatibility of peptide-coated chemical vapor deposited graphene interfaces with hippocampal neurons (polylysine-coated graphene[28]) or neural stem cells (laminin-coated graphene[30,31]). However, peptide coating might weaken neuron/interface electrical contacts and electrical signal transmission, resulting in nonoptimal charge transfer.[28,32−34]

METHODS

Multiwall Carbon Nanotubes Preparation. MWNT-coated substrates are prepared similarly to our previous refs 17−19 (optimized MWNT dispersion concentration 0.1 mg/mL; final MWNT film density $7 \times 10-5$ mg/mm^2). Briefly, MWNTs (Nanostructured & Amorphous Materials, Inc., Stock#: 1237YJS, outer diameter 20−30 nm), used as received, are functionalized using 1,3-dipolar cycloaddition. Ethyl acetate solution of functionalized MWNTs (0.1 mg/mL) is sprayed on glass coverslips placed on a hot plate at 200 °C, then the substrates are heated at 350 °C under nitrogen atmosphere to restore the pristine structure of MWNTs.

Electrical Characterization. A Jandel station with 4-Probe head, 100 μm titanium tips arranged in a straight line 1 mm apart, combined with a Keithley 2100 digital multimeter is used to measure R_s pre and post thermal annealing, avoiding sample edges, in order to verify the approximation of the four probe method.[68] The measurement accuracy is verified against a 12.93Ω/□ ITO on glass reference (Jandel Engineering Ltd., tested against a NIST traceable sample).

Scanning Electron Microscopy. GBSs and cellular adaption to substrates are qualitatively assessed through scanning electron microscopy (SEM). Images are acquired collecting secondary electrons on a Gemini SUPRA 40 SEM (Carl Zeiss NTS GmbH, Oberkochen, Germany) working at 5 keV. Cellular samples are washed with 0.1 M cacodylate buffer (pH = 7.2) and fixed with a solution containing 2% glutaraldehyde (Fluka, Italy) in 0.1 M cacodylate buffer for 1 h at room temperature. Cultures are then washed in a cacodylate buffer and dehydrated by dipping in water/ethanol solutions at progressively higher alcohol concentrations (50%, 75%, 95% and 100% ethanol for 3 min each). Samples are dried at room temperature in a N$_2$ chamber overnight. Prior to SEM imaging, samples are gold metalized in a metal sputter coater (Polaron SC7620).

Neuronal Cultures and Electrophysiology. Dissociated hippocampal neurons are obtained from postnatal (P2−P3) rats, as previously described.[16−18] For each culture series, sister cultures are prepared by plating cells on control substrates or on GBS-covered coverslips, and the

activity, synaptogenesis, and for their short-term synaptic plasticity and single-cell electro-genic properties[16,19] in the same in vitro models. The precise mechanisms determining the different impact on neuronal activity of these two carbon based substrates requires further investigation. Our data using CNTs control surfaces strengthens the hypothesis that the tight and intimate interactions among CNTs and neurons, combined with the conductivity,[17] are responsible for their ability to interfere with synaptic networks.[18,19] The lower roughness of GBSs (∼14 or ∼9 nm in GBSs against ∼30 nm in MWNT[18]), might

same number of cells (~30.000) is plated on each coverslip. Cultures are used for experiments over 8−10 days *in vitro*. Neuronal and glial cells densities are quantified by immunofluorescence stainings and microscopy analysis.[16,18,20] Cultures are fixed with 4% paraformaldehyde in phosphate buffer solution (PBS), incubated in blocking solution and stained by incubation with primary antibodies (against NeuN for neuronal staining, mouse monoclonal, 1:100, Millipore; or against glial fibrillary acidic protein (GFAP) for glial cells staining, mouse monoclonal, 1:400, Sigma). Upon washout in PBS, cultures are incubated with the secondary goat antibody (Alexa Fluor-488-conjugated; 1:500; Invitrogen) and with 4′,6-diamidino-2-phenylindole (DAPI) for nuclei staining. Samples are mounted in a Vectashield medium and images are acquired using a conventional epifluorescence microscope (Leica DM6000). Whole-cell patch clamp recordings are performed with pipettes filled with 120 mM K gluconate, 20 mM KCl, 10 mM HEPES, 2 mM MgCl$_2$, 4 mM MgATP, 0.3 mM GTP (pH adjusted to 7.35 with KOH). The external solution contains the following: 150 mM NaCl, 4 mM KCl, 1 mM MgCl$_2$, 2 mM CaCl$_2$, 10 mM HEPES, 10 mM glucose (pH adjusted to 7.4 with NaOH). Experiments are performed at room temperature. Recordings are taken with a Multiclamp 700B amplifier (Molecular Devices). Current and voltage clamp signals are digitized at 10 kHz by a Digidata 1440A equipped with the pCLAMP 10 software (Molecular Devices) and stored for analysis. Neuronal passive membrane properties are evaluated by applying a 10 mV hyperpolarizing step (250 ms). Dual recordings are taken by eliciting action potentials in the presynaptic cell (in current-clamp mode) by injecting short square current pulses (1 nA, 2 ms) at −60 mV resting membrane potential, and recording response postsynaptic currents from the postsynaptic cell voltage-clamped at −56 mV holding potential (potential values not corrected for 14 mV liquid junction potential). Paired-pulse ratio (PPR) analysis is performed on monosynaptically connected (latency between the peak of the elicited presynaptic action potential and the onset of the postsynaptic current response less than 3 ms) neuron pairs.[18] A pair of spikes at 20 Hz is induced in the presynaptic neurons (10−20 times repetitions at 10 s intervals) and currents evoked in the postsynaptic neurons are recorded (in our experimental setting the majority of postsynaptic currents observed in dual recordings are GABA-mediated, as in ref 18; GABAergic synapses are therefore analyzed). Recordings showing ongoing spontaneous activity occasionally superimposed to the evoked postsynaptic current are excluded from the analysis.

Statistics. Statistically significant differences between data sets are assessed by the Student's test (after validation of variances homogeneity by Levene's test) for parametric data and by Mann−Whitney for nonparametric ones.[69] For synaptic pairing, comparisons are performed by paired *t* tests between data sets obtained from sister cultures from the different culture series. A *p*-value < 0.05 is taken as indicative of statistically significant differences. *n* is the number of neurons, if not otherwise indicated. Data are shown as mean ± standard error of the mean.

Ethical Statement. The work on animals (neonatal rats) was performed according to the EU guidelines (2010/63/UE) and Italian law (decree 26/14). The use of animals was approved by the Italian Ministry of Health, in agreement with the EU Recommendation 2007/526/CE. Animals were hosted by the University of Trieste Animal Facility (Life Sciences Department, Italy, authorized by the Italian Ministry of Health), and breeding conditions and procedures complied with the 2010/63/UE EU guidelines and Italian law (26/14). Neonatal rats were sacrificed by rapid decapitation and the tissue of interest (hippocampus) was harvested; all efforts were made to minimize suffering. The work was performed on explanted tissue and did not require ethical approval. The entire procedure employed in the present study is in accordance with the regulations of the Italian Animal Welfare Act, with the relevant EU legislation and guidelines on the ethical use of animals and is approved by the local Authority Veterinary Service. The procedures were also in accordance with the ethical assessment established in the EU FP7-ICT-2013-FET-F GRAPHENE Flagship project (No. 604391).

AUTHOR INFORMATION

Corresponding Authors

*E-mail: laura.ballerini@sissa.it.
*E-mail: acf26@eng.cam.ac.uk.
*E-mail: prato@units.it.
*E-mail: ester.vazquez@uclm.es.

Notes

The authors declare no competing financial interest.

REFERENCES

(1) Kotov, N. A.; Winter, J. O.; Clements, I. P.; Jan, E.; Timko, B. P.; Campidelli, S.; Pathak, S.; Mazzatenta, A.; Lieber, C. M.; Prato, M.; Bellamkonda, R. V.; Silva, G. A.; Shi Kam, N. W.; Patolsky, F.; Ballerini, L. Nanomaterials for Neural Interfaces. *Adv. Mater.* **2009**, *21*, 3970−4004.

(2) Fattahi, P.; Yang, G.; Kim, G.; Abidian, M. R. A Review of Organic and Inorganic Biomaterials for Neural Interfaces. *Adv. Mater.* **2014**, *26*, 1846−1850.

(3) Benabid, A. L. Deep Brain Stimulation for Parkinson's Disease. *Curr. Opin. Neurobiol.* **2003**, *13*, 696−706.

(4) Bensmaia, S. J.; Miller, L. E. Restoring Sensorimotor Function through Intracortical Interfaces: Progress and Looming Challenges. *Nat. Rev. Neurosci.* **2014**, *15*, 313−325.

(5) Lebedev, M. A.; Nicolelis, M. A. Brain-Machine Interfaces: Past, Present and Future. *Trends Neurosci.* **2006**, *29*, 536−546.

(6) Karumbaiah, L.; Saxena, T.; Carlson, D.; Patil, K.; Patkar, R.; Gaupp, E. A.; Betancur, M.; Stanley, G. B.; Carin, L.; Bellamkonda, R. V. Relationship between Intracortical Electrode Design and Chronic Recording Function. *Biomaterials* **2013**, *34*, 8061−8074.

(7) Vallejo-Giraldo, C.; Kelly, A.; Biggs, M. J. Biofunctionalisation of electrically conducting polymers. *Drug Discovery Today* **2014**, *19*, 88−94.

(8) Mazzatenta, A.; Giugliano, M.; Campidelli, S.; Gambazzi, L.; Businaro, L.; Markram, H.; Prato, M.; Ballerini, L. Interfacing Neurons with Carbon Nanotubes: Electrical Signal Transfer and Synaptic Stimulation in Cultured Brain Circuits. *J. Neurosci.* **2007**, *27*, 6931−6936.

(9) Keefer, E. W.; Botterman, B. R.; Romero, M. I.; Rossi, A. F.; Gross, G. W. Carbon Nanotube Coating Improves Neuronal Recordings. *Nat. Nanotechnol.* **2008**, *3*, 434−439.

(10) Shoval, A.; Adams, C.; David-Pur, M.; Shein, M.; Hanein, Y.; Sernagor, E. Carbon Nanotube Electrodes for Effective Interfacing with Retinal Tissue. *Front. Neuroeng.* **2009**, *2*, 1−9.

(11) Tosun, Z.; McFetridge, P. S. A Composite SWNT-Collagen Matrix: Characterization and Preliminary Assessment as a Conductive Peripheral Nerve Regeneration Matrix. *J. Neural. Eng.* **2010**, *7*, 066002.

(12) Dvir, T.; Timko, B. P.; Kohane, D. S.; Langer, R. Nano-technological Strategies for Engineering Complex Tissues. *Nat. Nanotechnol.* 2011, 6, 13−22.

(13) Gelain, F.; Panseri, S.; Antonini, S.; Cunha, C.; Donega, M.; Lowery, J.; Taraballi, F.; Cerri, G.; Montagna, M.; Baldissera, F.; Vescovi, A. Transplantation of Nanostructured Composite Scaffolds Results in the Regeneration of Chronically Injured Spinal Cords. *ACS Nano* 2011, 5, 227−236.

(14) Fabbro, A.; Bosi, S.; Ballerini, L.; Prato, M. Carbon Nanotubes: Artificial Nanomaterials to engineer Single Neurons and Neuronal Networks. *ACS Chem. Neurosci.* 2012, 3, 611−618.

(15) Aregueta-Robles, U. A.; Woolley, A. J.; Poole-Warren, L. A.; Lovell, N. H.; Green, R. A. Organic Electrode Coatings for Next-Generation Neural Interfaces. *Front. Neuroeng.* 2014, 7 (15), 1−18.

(16) Lovat, V.; Pantarotto, D.; Lagostena, L.; Cacciari, B.; Grandolfo, M.; Righi, M.; Spalluto, G.; Prato, M.; Ballerini, L. Carbon Nanotube Substrates Boost Neuronal Electrical Signaling. *Nano Lett.* 2005, 5, 1107−1110.

(17) Cellot, G.; Cilia, E.; Cipollone, S.; Rancic, V.; Sucapane, A.; Giordani, S.; Gambazzi, L.; Markram, H.; Grandolfo, M.; Scaini, D.; Gelain, F.; Casalis, L.; Prato, M.; Giugliano, M.; Ballerini, L. Carbon Nanotubes Might Improve Neuronal Performance by Favoring Electrical Shortcuts. *Nat. Nanotechnol.* 2009, 4, 126−133.

(18) Cellot, G.; Toma, F. M.; Varley, Z. K.; Laishram, J.; Villari, A.; Quintana, M.; Cipollone, S.; Prato, M.; Ballerini, L. Carbon Nanotube Scaffolds Tune Synaptic Strength in Cultured Neural Circuits: Novel Frontiers in Nanomaterial-Tissue Interactions. *J. Neurosci.* 2011, 3, 12945−12953.

(19) Fabbro, A.; Villari, A.; Laishram, J.; Scaini, D.; Toma, F. M.; Turco, A.; Prato, M.; Ballerini, L. Spinal Cord Explants Use Carbon Nanotube Interfaces to Enhance Neurite Outgrowth and to Fortify Synaptic Inputs. *ACS Nano* 2012, 6, 2041−2055.

(20) Fabbro, A.; Sucapane, A.; Toma, F. M.; Calura, E.; Rizzetto, L.; Carrieri, C.; Roncaglia, P.; Martinelli, V.; Scaini, D.; Masten, L.; Turco, A.; Gustincich, S.; Prato, M.; Ballerini, L. Adhesion to Carbon Nanotube Conductive Scaffolds Forces Action-Potential Appearance in Immature Rat Spinal Neurons. *PLoS One* 2013, 8, e73621.

(21) Cullen, D. K.; Wolf, J. A.; Smith, D. H.; Pfister, B. J. Neural Tissue Engineering for Neuroregeneration and Biohybridized Interface Microsystems *in Vivo* (Part 2. *Crit Rev. Biomed Eng.* 2011, 39, 241−259.

(22) Geim, A. K.; Novoselov, K. S. The Rise of Graphene. *Nat. Mater.* 2007, 6, 183−191.

(23) Hess, L. H.; Seifert, M.; Garrido, J. A. Graphene Transistors for Bioelectronics. *Proc. IEEE* 2013, 101, 1780−1792.

(24) Sanchez, V. C.; Jachak, A.; Hurt, R. H.; Kane, A. B. Biological Interactions of Graphene-family Nanomaterials: an Interdisciplinary Review. *Chem. Res. Toxicol.* 2014, 25, 15−34.

(25) Bianco, A. Graphene: Safe or Toxic? The Two Faces of the Medal. *Angew. Chem., Int. Ed.* 2013, 52, 4986−4997.

(26) Nayak, T. R.; Andersen, H.; Makam, V. S.; Khaw, C.; Bae, S.; Xu, X.; Ee, P.-L. R.; Ahn, J.-H.; Hong, B. H.; Pastorin, G.; Özyilmaz, B. Graphene for Controlled and Accelerated Osteogenic Differentiation of Human Mesenchymal Stem Cells. *ACS Nano* 2011, 5, 4670−4678.

(27) Conroy, J.; Verma, N. K.; Smith, R. J.; Rezvani, E.; Duesberg, G. S.; Coleman, J. N.; Volkov, Y. Biocompatibility of Pristine Graphene Monolayers, Nanosheets and Thin Films 2014, arXiv:1406.2497 [q-bio.CB].

(28) Li, N.; Zhang, X.; Song, Q.; Su, R.; Zhang, Q.; Kong, T.; Liu, L.; Jin, G.; Tang, M.; Cheng, G. The Promotion of Neurite Sprouting and Outgrowth of Mouse Hippocampal Cells in Culture by Graphene Substrates. *Biomaterials* 2011, 32, 9374−9382.

(29) Bendali, A.; Hess, L. H.; Seifert, M.; Forster, V.; Stephan, A. F.; Garrido, J. A.; Picaud, S. Purified Neurons can Survive on Peptide-Free Graphene Layers. *Adv. Healthcare Mater.* 2013, 2, 929−933.

(30) Tang, M.; Song, Q.; Li, N.; Jiang, Z.; Huang, R.; Cheng, G. Enhancement of Electrical Signaling in Neural Networks on Graphene Films. *Biomaterials* 2013, 34, 6402−6411.

(31) Park, S. Y.; Park, J.; Sim, S. H.; Sung, M. G.; Kim, K. S.; Hong, B. H.; Hong, S. Enhanced Differentiation of Human Neural Stem Cells into Neurons on Graphene. *Adv. Mater.* 2011, 23, H263−267.

(32) Djilas, M.; Olès, C.; Lorach, H.; Bendali, A.; Dégardin, J.; Dubus, E.; Lissorgues-Bazin, G.; Rousseau, L.; Benosman, R.; Ieng, S.-H.; Joucla, S.; Yvert, B.; Bergonzo, P.; Sahel, J.; Picaud, S. Three-Dimensional Electrode Arrays for Retinal Prostheses: Modeling, Geometry Optimization and Experimental Validation. *J. Neural. Eng.* 2011, 8, 046020.

(33) Heim, M.; Rousseau, L.; Reculusa, S.; Urbanova, V.; Mazzocco, C.; Joucla, S.; Bouffier, L.; Vytras, K.; Bartlett, P.; Kuhn, A.; Yvert, B. Combined Macro-/Mesoporous Microelectrode Arrays for Low-Noise Extracellular Recording of Neural Networks. *J. Neurophysiol.* 2012, 108, 1793−1803.

(34) Heim, M.; Yvert, B.; Kuhn, A. Nanostructuration Strategies to Enhance Microelectrode Array (MEA) Performance for Neuronal Recording and Stimulation. *J. Physiol.* 2012, 106, 137−145.

(35) Novoselov, K. S.; Jiang, D.; Schedin, F.; Booth, T. J.; Khotkevich, V. V.; Morozov, S. V.; Geim, A. K. Two-Dimensional Atomic Crystals. *Proc. Natl. Acad. Sci. U. S. A.* 2005, 102, 10451−10453.

(36) Bonaccorso, F.; Lombardo, A.; Hasan, T.; Sun, Z.; Colombo, L.; Ferrari, A. C. Production and Processing of Graphene and 2D Crystals. *Mater. Today* 2012, 15, 564−589.

(37) Ferrari, A. C.; Bonaccorso, F.; Fal'Ko, V.; Novoselov, K. S.; Roche, S.; Boggild, P.; Borini, S.; Koppens, F. H. L.; Palermo, P.; Pugno, N.; Garrido, J. A.; Sordan, R.; Bianco, A.; Ballerini, L.; Prato, M.; Lidorikis, E.; Kivioja, J.; Marinelli, C.; Ryhänen, T.; Morpurgo, A.; et al. Science and Technology Roadmap for Graphene, Related Two-Dimensional Crystals, and Hybrid Systems. *Nanoscale* 2015, 7, 4598−4810.

(38) Bonaccorso, F.; Sun, Z.; Hasan, T.; Ferrari, A. C. Graphene Photonics and Optoelectronics. *Nat. Photonics* 2010, 4, 611−622.

(39) Bonaccorso, F.; Colombo, L.; Yu, G.; Stoller, M.; Tozzini, V.; Ferrari, A. C.; Ruoff, R. S.; Pellegrini, V. Graphene, Related Two Dimensional Crystals, and Hybrid Systems for Energy Conversion and Storage. *Science* 2015, 347, 1246501.

(40) Huang, X.; Yin, Z.; Wu, S.; Qi, X.; He, Q.; Zhang, Q.; Yan, Q.; Boey, F.; Zhang, H. Graphene-Based Materials: Synthesis, Character-ization, Properties, and Applications. *Small* 2011, 7, 1876−1902.

(41) Lipson, H.; Stokes, A. R. The Structure of Graphite. *Proc. R. Soc. London, Ser. A* 1942, 181, 101−105.

(42) N'Diaye, A. T.; Bleikamp, S.; Feibelman, P. J.; Michely, T. Two-Dimensional Ir Cluster Lattice on a Graphene Moiré on Ir(111). *Phys. Rev. Lett.* 2006, 97, 215501.

(43) Acheson, E. G. Manufacture of Graphite, U.S. Patent 615648, 1896.

(44) Forbeaux, I.; Themlin, J.-M.; Charrier, A.; Thibaudau, F.; Debever, J.-M. Solid-State Graphitization Mechanisms of Silicon Carbide 6H−Sic Polar Faces. *Appl. Surf. Sci.* 2000, 162, 406−412.

(45) Li, X.; Cai, W.; An, J.; Kim, S.; Nah, J.; Yang, D.; Piner, R.; Velamakanni, A.; Jung, I.; Tutuc, E.; Banerjee, S. K.; Colombo, L.; Ruoff, R. S. Large-Area Synthesis of High-Quality and Uniform Graphene Films on Copper Foils. *Science* 2009, 324, 1312−1314.

(46) Wang, L.; Meric, I.; Huang, P. Y.; Gao, Q.; Gao, Y.; Tran, H.; Taniguchi, T.; Watanabe, K.; Campos, L. M.; Muller, D. A.; Guo, J.; Kim, P.; Hone, J.; Shepard, K. L.; Dean, C. R. One-Dimensional Electrical Contact to a Two-Dimensional Material. *Science* 2013, 342, 614−617.

(47) Bae, S.; Kim, H.; Lee, Y.; Xu, X.; Park, J. S.; Zheng, Y.; Balakrishnan, J.; Lei, T.; Kim, H. R.; Song, Y. I.; Kim, Y. J.; Kim, K. S.; Özyilmaz, B.; Ahn, J. H.; Hong, B. H.; Iijima, S. Roll-To-Roll Production of 30-Inch Graphene Films for Transparent Electrodes. *Nat. Nanotechnol.* 2010, 5, 574−578.

(48) Brodie, B. C. Sur le Poids Atomique du Graphite. *Ann. Chim. Phys.* 1860, 59 (466), e472.

(49) Hummers, W. S.; Offeman, R. E. Preparation of Graphitic Oxide. *J. Am. Chem. Soc.* 1958, 80, 1339−1339.

(50) Mattevi, C.; Eda, G.; Agnoli, S.; Miller, S.; Mkhoyan, K. A.; Celik, O.; Mastrogiovanni, D.; Granozzi, G.; Garfunkel, E.; Chhowalla, M. Evolution of Electrical, Chemical, and Structural Properties of Transparent and Conducting Chemically Derived Graphene Thin Films. *Adv. Funct. Mater.* **2009**, *19*, 2577−2583.

(51) Eda, G.; Lin, Y. Y.; Mattevi, C.; Yamaguchi, H.; Chen, H. A.; Chen, I.; Chen, C. W.; Chhowalla, M. Blue Photoluminescence from Chemically Derived Graphene Oxide. *Adv. Mater.* **2010**, *22*, 505−509.

(52) Hernandez, Y.; Nicolosi, V.; Lotya, M.; Blighe, F. M.; Sun, Z.; De, S.; McGovern, I. T.; Holland, B.; Byrne, M.; Gun'ko, Y. K.; Boland, J. J.; Niraj, P.; Duesberg, G.; Krishnamurthy, S.; Goodhue, R.; Hutchison, J.; Scardaci, V.; Ferrari, A. C.; Coleman, J. N. High-Yield Production of Graphene by Liquid-Phase Exfoliation of Graphite. *Nat. Nanotechnol.* **2008**, *3*, 563−568.

(53) Hassoun, J.; Bonaccorso, F.; Agostini, M.; Angelucci, M.; Betti, M. G.; Cingolani, R.; Gemmi, M.; Mariani, C.; Panero, S.; Pellegrini, V.; Scrosati, B. An Advanced Lithium-Ion Battery Based on a Graphene Anode and a Lithium Iron Phosphate Cathode. *Nano Lett.* **2014**, *14*, 4901−4906.

(54) Torrisi, F.; Hasan, T.; Wu, W.; Sun, Z.; Lombardo, A.; Kulmala, T. S.; Hsieh, G.-W.; Jung, S.; Bonaccorso, F.; Paul, P. J.; Chu, D.; Ferrari, A. C. Inkjet-Printed Graphene Electronics. *ACS Nano* **2012**, *6*, 2992−3006.

(55) León, V.; Quintana, M.; Herrero, M. A.; Fierro, J. L. G.; de la Hoz, A.; Prato, M.; Vázquez, E. Few-Layer Graphenes from Ball-Milling of Graphite with Melamine. *Chem. Commun.* **2011**, *47*, 10936−10938.

(56) León, V.; Rodriguez, A. M.; Prieto, P.; Prato, M.; Vázquez, E. Exfoliation of Graphite with Triazine Derivatives under Ball-Milling Conditions: Preparation of Few-Layer Graphene *via* Selective Noncovalent Interactions. *ACS Nano* **2014**, *8*, 563−571.

(57) Maragó, O. M.; Bonaccorso, F.; Saija, R.; Privitera, G.; Gucciardi, P. G.; Iatì, M. A.; Calogero, G.; Jones, P. H.; Borghese, F.; Denti, P.; Nicolosi, V.; Ferrari, A. C. Brownian Motion of Graphene. *ACS Nano* **2010**, *4*, 7515−7523.

(58) Sun, Z.; Hasan, T.; Torrisi, F.; Popa, D.; Privitera, G.; Wang, F.; Bonaccorso, F.; Basko, D. M.; Ferrari, A. C. Graphene Mode-Locked Ultrafast Laser. *ACS Nano* **2010**, *4*, 803−810.

(59) Schwartzkroin, P. A. Further Characteristics of Hippocampal CA 1 Cells *in Vitro*. *Brain Res.* **1977**, *128*, 53−68.

(60) Kravets, V. G.; Grigorenko, A. N.; Nair, R. R.; Blake, P.; Anissimova, S.; Novoselov, K. S.; Geim, A. K. Spectroscopic Ellipsometry of Graphene and an Exciton-Shifted Van Hove Peak in Absorption. *Phys. Rev. B: Condens. Matter Mater. Phys.* **2010**, *81*, 155413.

(61) Ferrari, A. C.; Basko, D. M. Raman Spectroscopy as a Versatile Tool for Studying the Properties of Graphene. *Nat. Nanotechnol.* **2014**, *8*, 235−246.

(62) Ferrari, A. C.; Meyer, J. C.; Scardaci, V.; Casiraghi, C.; Lazzeri, M.; Mauri, F.; Piscanec, S.; Jiang, D.; Novoselov, K. S.; Roth, S.; Geim, A. K. Raman Spectrum Of Graphene and Graphene Layers. *Phys. Rev. Lett.* **2006**, *97*, 187401.

(63) Ferrari, A. C.; Robertson, J. Interpretation of Raman Spectra of Disordered and Amorphous Carbon. *Phys. Rev. B: Condens. Matter Mater. Phys.* **2000**, *61*, 14095.

(64) Ferrari, A. C.; Robertson, J. Resonant Raman Spectroscopy of Disordered, Amorphous, and Diamondlike Carbon. *Phys. Rev. B: Condens. Matter Mater. Phys.* **2001**, *64*, 075414.

(65) Casiraghi, C.; Hartschuh, A.; Qian, H.; Piscanec, S.; Georgi, C.; Fasoli, A.; Novoselov, K. S.; Basko, D. M.; Ferrari, A. C. Raman Spectroscopy of Graphene Edges. *Nano Lett.* **2009**, *9*, 1433−1449.

(66) Korkut, S.; Roy-Mayhew, J. D.; Dabbs, D. M.; Milius, D. L.; Aksay, I. A. High Surface Area Tapes Produced with Functionalized Graphene. *ACS Nano* **2011**, *5*, 5214−5222.

(67) Nečas, D.; Klapetek, P. Gwyddion: An Open-Source Software for SPM Data Analysis. *Cent. Eur. J. Phys.* **2012**, *10*, 181−188.

(68) Smits, F. M. Measurement of Sheet Resistivities with the Four-Point Probe. *Bell Syst. Tech. J.* **1958**, *37*, 711−718.

(69) Fabbro, A.; Villari, A.; Laishram, J.; Scaini, D.; Toma, F. M.; Turco, A.; Prato, M.; Ballerini, L. Spinal Cord Explants Use Carbon Nanotube Interfaces to Enhance Neurite Outgrowth and to Fortify Synaptic Inputs. *ACS Nano* **2012**, *6*, 2041−2055.